CARDIFF UNIVERSITY
PRIFYSGOL CAERDYDD

ORCA – Online Research @ Cardiff

This is an Open Access document downloaded from ORCA, Cardiff University's institutional repository:https://orca.cardiff.ac.uk/id/eprint/126468/

This is the author's version of a work that was submitted to / accepted for publication.

Citation for final published version:

Chen, Andrew, Juang, Bor-Chau, Ren, Dingkun, Liang, Baolai, Prout, David L., Chatziioannou, Arion F. and Huffaker, Diana L. 2019. Significant suppression of surface leakage in GaSb/AlAsSb heterostructure with Al2O3 passivation. Japanese Journal of Applied Physics 58 (9) , 090907. 10.7567/1347-4065/ab3909

Publishers page: http://dx.doi.org/10.7567/1347-4065/ab3909

Please note:
Changes made as a result of publishing processes such as copy-editing, formatting and page numbers may not be reflected in this version. For the definitive version of this publication, please refer to the published source. You are advised to consult the publisher's version if you wish to cite this paper.

This version is being made available in accordance with publisher policies. See http://orca.cf.ac.uk/policies.html for usage policies. Copyright and moral rights for publications made available in ORCA are retained by the copyright holders.

1
2
3
4
5
6
7
8
9
10
11
12
13
14
15
16
17
18
19
20
21
22
23
24
25
26
27
28
29
30
31
32
33
34
35
36
37
38
39
40
41
42
43
44
45
46
47
48
49
50
51
52
53
54
55
56
57
58
59
60

Significant Suppression of Surface Leakage in GaSb/AlAsSb Heterostructure with Al_2O_3 Passivation

Andrew Chen[1], Bor-Chau Juang[1], Dingkun Ren[1], Baolai Liang[2]*, David L. Prout[3], Arion F. Chatziioannou[3], and Diana L. Huffaker[1]

[1]*Department of Electrical and Computer Engineering, University of California - Los Angeles, CA 90095, USA.*

[2]*California NanoSystems Institute, University of California - Los Angeles, CA 90095, USA*

[3]*Department of Medical and Molecular Pharmacology, University of California - Los Angeles, CA 90095, USA*

* E-mail: bliang@cnsi.ucla.edu

This work develops a $(NH_4)_2S/Al_2O_3$ passivation technique for photodiode-based GaSb/AlAsSb heterostructure. Surface-sulfurated GaSb/AlAsSb heterostructure mesas show a significant suppression of reversed-bias dark current by 4 – 5 orders of magnitude after they are further passivated by Al_2O_3 layers. So the mesa sidewalls treated with $(NH_4)_2S/Al_2O_3$ layers can effectively inhibit the shunt path of dark carriers. The activation energies for both bulk and surface components are extracted from temperature-dependent current-voltage characteristics, which suggest that the bulk characteristics remain unchanged, while Fermi-level pinning at surfaces is alleviated. Additionally, temperature coefficients of the breakdown voltage are extracted, confirming that the breakdown process is confined entirely in the large bandgap AlAsSb regions. This study shows that the implementation of $(NH_4)_2S/Al_2O_3$ passivation can lead to room-temperature GaSb-based photodiodes and GaSb/AlAsSb-based avalanche photodiodes for highly efficient photodetection.

.

Gallium antimonide (GaSb), a compound III-V semiconductor material with bandgap of 0.726 eV (or equivalent absorption wavelength ~1.71 μm) at room temperature, has been implemented into a variety of photodetectors at short-, mid-, and long-wavelength infrared regimes.[1-5] To fabricate pixels, i.e., focal plane arrays, bulk GaSb materials are typically etched by chemicals into mesa shapes with exposed GaSb surfaces (or GaSb/air interfaces). It is known that nonradiative recombination centers on surfaces, i.e., surface states (or dangling bonds), which are caused by interruptions to the crystal periodicity, can lead to high leakage current at reverse bias and thus poor signal-to-noise ratio. To minimize this effect, it is critical to properly passivate surfaces using chemicals or dielectric layers to prevent sidewalls from being re-oxidized. Unfortunately, many studies have shown that improving surface quality for antimony-based (Sb-based) material systems is challenging due to the complex combination of native oxides on their surfaces.[6-9] This is because the exposed mesa sidewall tends to form a thin layer of native oxide (e.g. Ga_2O_3 and Sb_2O_3 through $2GaSb + 3O_2 \rightarrow Ga_2O_3 + Sb_2O_3$), and a layer of elemental antimony (Sb) is normally observed at the interface between bulk GaSb and its native oxide, resulting in a shunt path for carriers.[10] Thus, a crucial step in the fabrication is to develop a robust and controllable passivation technique for the etched GaSb surfaces.

To date, a wide range of surface passivation methods (i.e., ammonium sulfide $(NH_4)_2S$,[11-13] SiO_2,[15,16] SiN_x,[16] polyamide,[17] and overgrowth with large bandgap material[18]) have been reported for fabrication of Sb containing photodetectors. Among these techniques, sulfuration and SiO_2 deposition are the most common. $(NH_4)_2S$ solution (with varied dilution ratios) can etch off the native oxides and saturate dangling bonds. In our study, however, we observed that the dark current density of GaSb-based detectors after $(NH_4)_2S$ treatment remains relatively high at room temperature (~6×10^{-4} A/cm^2 at reverse bias of 5 V) and increases with decreasing mesa size, which suggests that surface leakage current is still prominent.[19] Furthermore, the treated GaSb surfaces tend to degrade over time as the sulfur atoms gradually desorb.[14,19] These observations suggest that the $(NH_4)_2S$ passivation technique is unstable and needs to be further developed. On the other hand, passivation using SiO_2 is promising because the layer thickness can be freely controlled by the deposition time while such a dielectric layer can prevent the desorption of sulfur. However, the SiO_2 deposition process normally requires high temperature (or high radio-frequency power) to excite plasma, which can damage the material surface quality and introduce additional dangling bonds or surface states.

To overcome these issues, we optimize the surface passivation for GaSb using a

combination of $(NH_4)_2S$ and conformal Al_2O_3 layer by atomic-layer deposition (ALD). The ALD technique is plasma-free and is conducted at low temperature (~200 °C). Moreover, it has been discovered that Al_2O_3 can suppress the formation of native oxide on III-V material surfaces during deposition due to lower Gibbs free energy (-377.9 kcal/mol).[13,20] This value is lower than the Gibbs free energies of Sb_2O_3, Ga_2O, Ga_2O_3, As_2O_3 and As_2O_5, which are -151.5 kcal/mol, -75.3 kcal/mol, -238.6 kcal/mol, -137.7 kcal/mol and -187.0 kcal/mol, respectively.[13,21] In addition, the electrical characterization of GaSb-based metal–oxide–semiconductor capacitors has showcased successful elimination of Sb_2O_3 after Al_2O_3 deposition.[13,22] Here we introduce a sulfurized surface with Al_2O_3 passivation to our GaSb/AlAsSb mesa heterostructures. Such heterostructures are based on our previously studied GaSb/AlAsSb separate absorption and multiplication avalanche photodiodes (SAM-APDs).[23] We observe a significant suppression of dark current at reverse bias, and a remarkable improvement of avalanche breakdown, both at room temperature. To understand the underlying physics, we further extract activation energies and breakdown temperature coefficients. We observe a remarkable difference in surface-related activation energies from devices with and without Al_2O_3, while the activation energies from bulk materials remain almost constant. This clearly suggests that the surface passivation plays an important role in modulating surface quality and device characteristics. This study paves the way to room-temperature GaSb-based photodiodes and GaSb/AlAsSb-based avalanche photodiodes for highly efficient photodetection.

Figure 1 shows a schematic of the GaSb/AlAsSb heterostructure with Al_2O_3 passivation, which is composed of both small bandgap GaSb and large bandgap $AlAs_{0.08}Sb_{0.92}$ PIN regions. Such heterostructures were developed based on our previous study on GaSb PIN diodes and GaSb/AlAsSb SAM-APDs for energy-sensitive photodetection, along with a series of detector characterizations, which include current-voltage (I-V), capacitance-voltage (C-V), photo-response, radiation response, among others.[19,23-25] The AlAsSb region was lattice-matched to the GaSb region, grown by molecular beam epitaxy (MBE) on an *n*-type GaSb substrate.[23,25] Tellurium and Beryllium were used as *n*-type and *p*-type dopants, respectively. The growth was started with the multiplication region. An $AlAs_{0.08}Sb0_{.92}$ PIN junction (digital-alloy) with a *p*-AlAsSb field-control layer (1×10^{17} cm^{-3}) was first formed, followed by the growth of a 2 µm un-doped GaSb absorber. The GaSb absorption region was capped by a 50 nm large bandgap *p*-$Al_{0.4}Ga_{0.6}Sb$ window layer (7×10^{18} cm^{-3}), followed by growth of 50 nm highly-doped *p*-GaSb atop as ohmic contact (1×10^{18} cm^{-3}). In this GaSb/AlAsSb heterostructure, the majority of the electric field can be tightly confined within the

large bandgap AlAsSb multiplication region, which can minimize the dark current from Shockley–Read–Hall nonradiative recombination and band-to-band tunneling.

After the MBE growth, the devices were fabricated into circular mesas of five sizes (d = 25 μm, 50 μm, 100 μm, 200 μm, and 400 μm) by standard photolithography using inductively coupled plasma etcher (BCl_3/Ar). The etching method was chosen by the fact that it gives the lowest possible dark current floor among the available approaches. Then, the samples were submerged in a $(NH_4)_2S$ solution for 15 minutes, i.e., sulfuration, as the first step of surface passivation. The dilution ratio was $(NH_4)_2S$:H_2O = 1:4. Next, the samples were blow-dried by nitrogen (without rinsing with deionized water) and quickly transferred into the ALD system (Cambridge Nanotech Fiji F200). A ~30 nm thick thermal Al_2O_3 layer (300 cycles with ~1 Å/cycle) was deposited at 200 °C (substrate temperature). During deposition, 0.06 sccm trimethylaluminum (TMA) and 0.06 sccm water vapor (H_2O) pulses were delivered into the chamber in a sequential fashion under a constant nitrogen flow of 20 sccm. To take away any by-products, a wait time of 10 sec was added between two neighboring cycles. Note that both TMA and H_2O were unheated. Finally, the Al_2O_3-passivated devices were etched by buffered oxide etch (BOE) to expose both top and bottom contacts. The etch rate on Al_2O_3 was calibrated to 1 nm/sec. Using BOE instead of concentrated hydrofluoric (HF) acid (49%) can result in better etch profiles since concentrated HF is corrosive to photoresist.[26)]

The Al_2O_3 ALD deposition mechanism has been previously studied.[27,28)] During sequential deposition cycles, the TMA and H_2O precursors react with the gas molecules, which are adsorbed on the device surfaces at the previous stage. Compared with other dielectric deposition techniques, ALD can achieve higher-quality GaSb surfaces due to several reasons, for example: (1) a precise control of deposition thickness at atomic level (since the thickness only depends on the number of cycles), (2) ideal conformal coverage, and (3) large area thickness uniformity. Equipped with these properties and the fact that Al_2O_3 formation is energetically favorable for GaSb over other dielectrics, Al_2O_3 by ALD deposition was the preferred option.

It is extremely critical to cap sulfurated GaSb/AlAsSb surfaces by Al_2O_3 layer to achieve optimized surface quality. We surmise that sulfur treatment followed by Al_2O_3 capping changed the dielectric environment, as in the case of passivation for III-AsSb.[29, 30)] The sulfur etched the native Al, Ga, As, and Sb oxides on the surface and passivated the dangling bonds.[31-33)] Any remaining native oxides formed following the sulfur treatment or sulfur desorption can be further etched by the ALD precursor (i.e., TMA). As a result, we

hypothesize two possible reasons why Al_2O_3 improves passivation: (1) Al-O participates in interfacial bonding through supplementing or substituting sulfur terminated bonds,[33] and (2) Al_2O_3 shells prevent desorption of sulfur atoms from the detector surface.

The room-temperature I-V characteristics at different passivation stages are shown in Figure 2(a) with a constant mesa diameter d of 200 μm. The $(NH_4)_2S/Al_2O_3$ passivation results an over 4-order reduction of dark current compared with that of the as-fab device (without any passivation), while the passivation with only $(NH_4)_2S$ treatment gives about 3-order reduction. Interestingly, electrical breakdown is only observed at room temperature for the case of $(NH_4)_2S/Al_2O_3$. This suggests that Al_2O_3 layers offer good insulation and lower dark current floor by suppressing the surface leakage current. We further examine the dark current density of the Al_2O_3-passivated devices with varied d, as shown in Figure 2(b). Clearly, the dark current density increases with decreasing d below the breakdown voltage (V_{BD}), which means that at high reverse bias the surface leakage current remains significant regardless of surface passivation.

The temperature-dependent I-V characteristics are further studied. We first select two devices with d of 100 μm and 200 μm and investigate the impact of surface passivation on their reverse leakage current at liquid-nitrogen cooled temperature, i.e., 77 K. As shown in Figure 3, capping Al_2O_3 layers on sulfurated GaSb surfaces offers an additional reduction of leakage current by 2 – 3 orders of magnitude around V_{BD} (~27 V). It should be noted that V_{BD} does not show a significant variation, which indicates that the bulk material properties remain the same regardless of passivation with or without Al_2O_3 layers. The noise level of the I-V measurement setup is on the order of 10^{-13} A.

As shown in Figure 4(a), a strong dependence of the dark current on temperature is observed with no abrupt increase before breakdown, which indicates that band-to-band-tunneling (BTBT) current from both AlAsSb and GaSb regions is negligible. To analyze the activation energy, the total dark current density (I_{total}) is decoupled into two components, and can be described as

$$J_{total} = J_{bulk} + J_{surface} \times \frac{P}{A} \qquad (1)$$

where J_{bulk} (A/cm^2)is the current density from the bulk material, $J_{surface}$ (A/cm) is the current density from the surface leakage, A (cm^2) is the device area (i.e., mesa size), and P (cm) is the mesa perimeter. With the decoupled J_{bulk} and $J_{surface}$ at different temperatures (77 K – 320 K) at a given bias (-0.1 V is chosen here for minimized field effect), their respective activation energies can be fitted using the following Arrhenius model:

1
2
3
4
5
6
7
8
9
10
11
12
13
14
15
16
17
18
19
20
21
22
23
24
25
26
27
28
29
30
31
32
33
34
35
36
37
38
39
40
41
42
43
44
45
46
47
48
49
50
51
52
53
54
55
56
57
58
59
60

$$J \propto T^{\frac{3}{2}} \times \exp\left(\frac{-E_a}{kT}\right) \qquad (2)$$

where T is temperature, k is the Boltzmann constant and E_a is the activation energy. Figure 4(b) shows the Arrhenius plots of bulk current from GaSb devices with and without Al_2O_3 passivation. The extracted energies are 0.297 eV and 0.304 eV, respectively. The nearly identical activation energies indicate that there is no degradation of the bulk materials after Al_2O_3 passivation. In contrast, the Al_2O_3-passivated device shows a surface activation energy of 0.178 eV, about 30% higher than that of the device with only $(NH_4)_2S$ passivation (0.132 eV) as shown in Figure 4(c). This result suggests that surface conduction is significantly suppressed and Fermi-level pinning is effectively alleviated in the Al_2O_3-passivated devices.

Last but not least, the temperature coefficients of breakdown voltage (C_{bd}) are extracted for the GaSb/AlAsSb heterostructures with and without Al_2O_3 passivation, yielding 17.4±0.5 mV/K and 16.51±1.9 mV/K, respectively. Positive value of C_{bd} suggests that the dominant breakdown mechanism is the avalanche process. No significant increment of dark current is observed before the breakdown (Figure 2 (b)), suggesting the breakdown process takes place only in the AlAsSb PIN regions. This observation agrees with the result from our previously shown GaSb/AlGaSb SAM-APDs, i.e., the electric field is entirely confined in the large bandgap AlAsSb regions thanks to the SAM structure.[23)] Conversely, if the breakdown event takes place in the small bandgap GaSb regions, an abrupt increment in dark current from BTBT would occur. In addition, the comparable C_{bd} regardless of the passivation treatment is likely due to the fact that C_{bd} is an intrinsic bulk characteristic and not affected by the surface conditions.

In conclusion, a $(NH_4)_2S/Al_2O_3$ passivation technique is developed and evaluated for the GaSb/AlAsSb heterostructures with different mesa sizes. We observed a significant suppression of dark current at reverse bias as well as an improved avalanche breakdown at room temperature. The activation energies were extracted from temperature-dependent I-V characteristics for both bulk and surface components. The results suggest that the bulk characteristics were not affected by the passivation process, while the surface conduction was significantly suppressed and Fermi-level pinning was effectively alleviated after the passivation process. Additionally, temperature coefficients of breakdown voltage were studied, which shows the breakdown process was confined entirely in the multiplication regions thanks to the SAM structure. This work provides an effective passivation technique to achieve room-temperature GaSb-based photodiodes and SAM-APDs for high-efficiency photodetection with significant applications in both industrial and research settings.

1
2
3
4
5
6
7
8
9
10
11
12
13
14
15
16
17
18
19
20
21
22
23
24
25
26
27
28
29
30
31
32
33
34
35
36
37
38
39
40
41
42
43
44
45
46
47
48
49
50
51
52
53
54
55
56
57
58
59
60

Acknowledgments

The authors acknowledge the financial support from the National Science Foundation (ECCS-1810507) and Defense Threat Reduction Agency (HDTRA1-14-1-0035).

References

1) A. Chavan, A. Chandola, S. Sridaran, and P. Dutta, *J. Appl. Phys.***100**, 064512 (2006).
2) S. Sridaran, A. Chavan, P. S. Dutta, *J. Cryst. Growth* **310**, 1590 (2008).
3) A. Rogalski, P. Martyniuk, and M. Kopytko, *Appl. Phys. Rev.* **4**, 031304 (2017).
4) M. Ren, S. Maddox, Y. Chen, M. Woodson, J. C. Campbell, and S. Bank, *Appl. Phys. Lett.* **108**, 081101 (2016).
5) C. G. Burguete, D. Guo, P. Jurczak, F. Cui, M. Tang, W. Chen, Z. Deng, Y. Chen, M. Gutiérrez, B. Chen, H. Liu, J. Wu, *IET Optoelectron.* **12**, 2 (2018).
6) G. P. Schwartz, *Thin Solid Films* **103**, 3 (1983).
7) S. Y. Xie, X.X. Zhou, S. Y. Zhang, D. J. Thomson, X. Chen, G.T. Reed, J. S. Ng, C. H. Tan, *Opt. Express* **24**, 24242 (2016)
8) J. L. Huang, W.Q. Ma, Y. L. Cao, Y. Wei, Y. H. Zhang, K. Cui, G. R. Deng, and Y. L. Shi, *Japanese Journal of Applied Physics* **51**, 074002 (2012).
9) J.-S. Liu, M. Clavel, and M. K. Hudait, *ACS Appl. Mater. Interfaces* **7**, 28624 (2015).
10) G. P. Schwartz, G.J. Gualtieri, J.E. Griffiths, C.D. Thurmond, and B. Schwartz, *J. Electrochem. Soc.* **127**, 2488 (1980).
11) V. N. Bessolov and M. V. Lebedev, *Semiconductors*. **32**, 1141 (1998).
12) E. Plis, J. B. Rodriguez, S. J. Lee, and S. Krishna, *Electron Lett.* **42**, 1248 (2006).
13) O. Salihoglu, A. Muti, K. Kutluer, T. Tansel, R. Turan, C. Kocabas, and A. Aydinli, *J. Appl. Phys.* **111**, 074509 (2012).
14) A. Gin, Y. Wei, A. Hood, A. Bajowala, V. Yazdanpanah, and M. Razeghi, *Appl. Phys. Lett.* **84**, 2037 (2004).
15) A. Gin, Y. Wei, J. Bae, A. Hood, J. Nah, and M. Razeghi, *Thin Solid Films* **447–448**, 489 (2004).
16) T. Tansel, K. Kutluer, Ö. Salihoglu, A. Aydinli, B. Aslan, B. Arikan, M. C. Kilinc, Y. Ergun, U. Serincan, and R. Turan, *IEEE Photon. Technol. Lett.* **24**, 790 (2012).
17) A. Hood, P. Y. Delaunay, D. Hoffman, M. Razeghi, and V. Nathan, *Appl. Phys. Lett.* **90**, 233513 (2007).

1
2
3
4
5
6
7
8
9
10
11
12
13
14
15
16
17
18
19
20
21
22
23
24
25
26
27
28
29
30
31
32
33
34
35
36
37
38
39
40
41
42
43
44
45
46
47
48
49
50
51
52
53
54
55
56
57
58
59
60

18) R. Rehm, M. Walter, F. Fuchs, J. Schmitz, and J. Fleissner, *Appl. Phys. Lett.* **86**, 173501 (2005).

19) B.-C. Juang, Ph.D. dissertation, University of California, Los Angeles, 2018.

20) D. Pulver, C. W. Wilmsen, D. Niles, and R. Kee, *J. Vac. Sci. Technol. B* **19**, 207 (2001).

21) G. Hollinger, R. S. Kabbani, and M. Gendry. *Phys. Rev. B.* **49**, 11159 (1994).

22) A. Ali, H. S. Madan, A. P. Kirk, D. A. Zhao, D. A. Mourey, M. K. Hudait, R. M. Wallace, T. N. Jackson, B. R. Bennett, J. B. Boos, and S. Datta, *Appl. Phys. Lett.* **97**, 143502 (2010).

23) B.-C. Juang, A. Chen, D. Ren, B. Liang, D. L. Prout, A. F. Chatziioannou, and D. L. Huffaker, *Adv. Optical Mater.***7**, 1900107 (2019).

24) B.-C. Juang, D. L. Prout, B. Liang, A. F. Chatziioannou, and D. L. Huffaker, Appl. Phys. Express **9**, 086401 (2016).

25) B.-C. Juang, B. Liang, D. Ren, D. L. Prout, A. F. Chatziioannou, and D. L. Huffaker, *Crystals* **7**, 313 (2017).

26) K. R. Williams and R. S. Muller, *J. Microelectromech. Syst.* **5**, 256 (1996).

27) M. D. Groner, F. H. Fabreguette, J. W. Elam, and S. M. George, *Chem. Mater.* **16**, 639 (2004).

28) S. M. George, *Chem. Rev.* **110**, 111 (2010).

29) D. Ren, Z. Rong, K. M. Azizur-Rahman, S. Somasundaram, M. Shahili, and D. L Huffaker, *Nanotechnology* **30**, 044002 (2019).

30) D. Ren, K. M. Azizur-Rahman, Z. Rong, B.-C. Juang, S. Somasundaram, M. Shahili, A. C. Farrell, B. S. Williams, and D. L Huffaker, *Nano Lett.***19**(5), 2793 (2019).

31) H. Oigawa, J.-F. Fan, Y. Nannichi, H. Sugahara, and M. Oshima, *Jpn. J. App. Phys.* **30**(3A), L322 (1991).

32) R. Driad, Z. H. Lu, S. Charbonneau, W. R. McKinnon, S. Laframboise, P. J. Poole, and S. P. McAlister, *App. Phys. Lett.* **73**, 665 (1998).

33) A. Higuera-Rodriguez, B. Romeira, S. Birindelli, L. E. Black, E. Smalbrugge, P. J. van Veldhoven, W. M. M. Kessels, M. K. Smit, and A. Fiore, *Nano Lett.* **17**, 2627 (2017).

1 2 3 4 5 6 7 8 9 10 11 12 13 14 15 16 17 18 19 20 21 22 23 24 25 26 27 28 29 30 31 32 33 34 35 36 37 38 39 40 41 42 43 44 45 46 47 48 49 50 51 52 53 54 55 56 57 58 59 60

Figure Captions

FIG. 1. Schematic of GaSb/AlAsSb heterostructure mesa passivated with a 30 nm Al_2O_3 film.

FIG. 2. Electrical characterizations at room temperature (295 K). (a) I-V characteristics of the GaSb/AlAsSb device at different stages of passivation; (b) J-V characteristics of the Al_2O_3-passivated GaSb/AlAsSb devices with different mesa sizes.

FIG. 3. Electrical characterizations at low temperature (77 K). I-V characteristics of passivated and unpassivated GaSb/AlAsSb devices with two different mesa sizes of 100 μm and 200 μm.

FIG. 4. Study of activation energies. (a) Temperature-dependent I-V characteristics of the Al_2O_3-passivated GaSb/AlAsSb device with mesa size of 200 μm; (b) Arrhenius plots for dark current contributed by the bulk materials; (c) Arrhenius plots for dark current contributed by the surface leakage.

Fig. 1

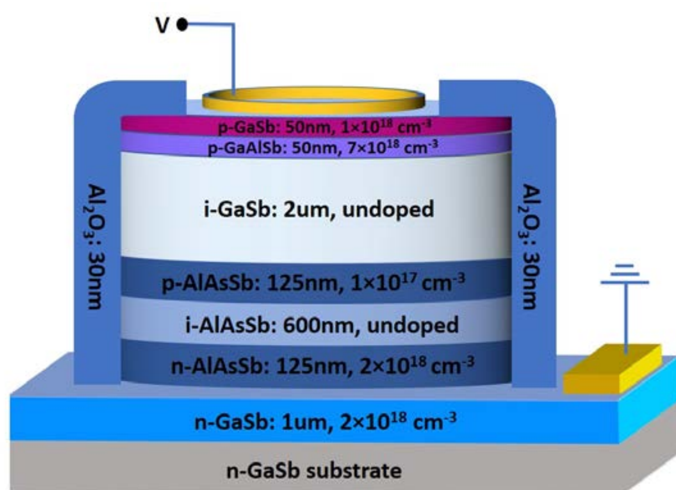

1
2
3
4
5
6
7
8
9
10
11
12
13
14
15
16
17
18
19
20
21
22
23
24
25
26
27
28
29
30
31
32
33
34
35
36
37
38
39
40
41
42
43
44
45
46
47
48
49
50
51
52
53
54
55
56
57
58
59
60

Fig. 2

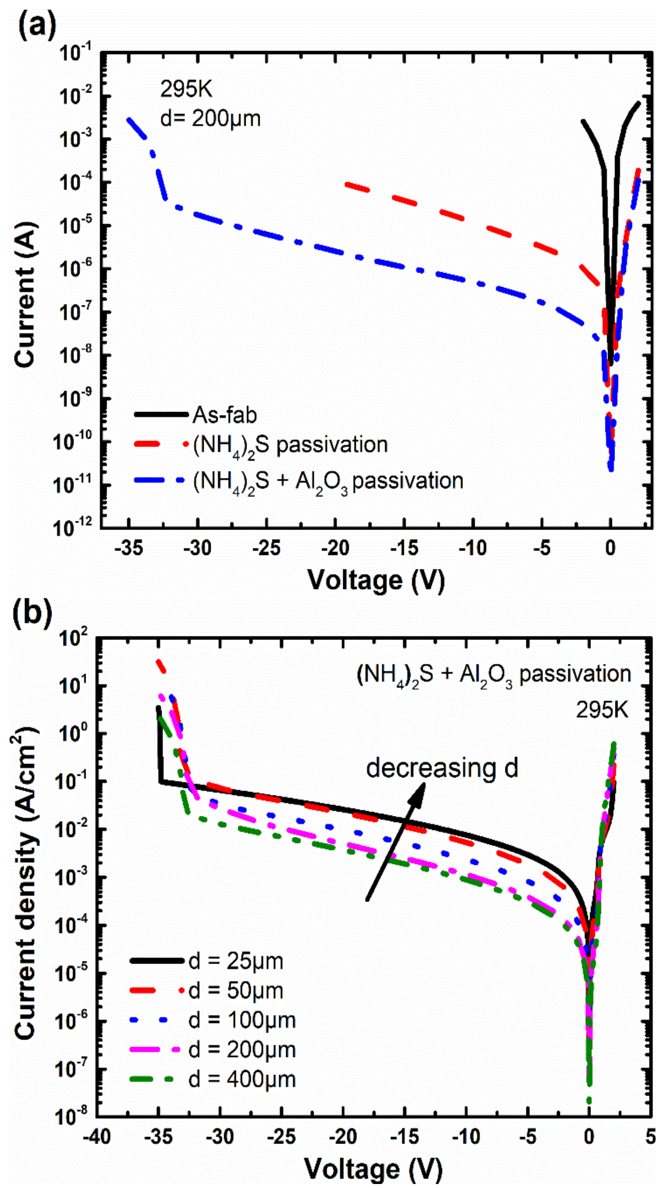

1
2
3
4
5
6
7
8
9
10
11
12
13
14
15
16
17
18
19
20
21
22
23
24
25
26
27
28
29
30
31
32
33
34
35
36
37
38
39
40
41
42
43
44
45
46
47
48
49
50
51
52
53
54
55
56
57
58
59
60

Fig. 3

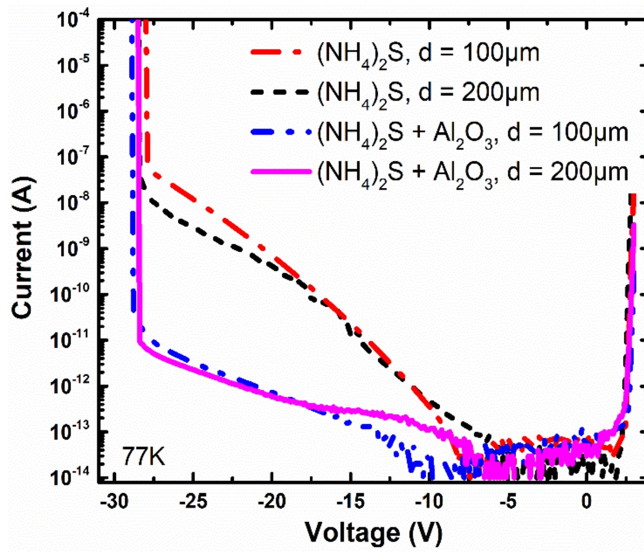

1
2
3
4
5
6
7
8
9
10
11
12
13
14
15
16
17
18
19
20
21
22
23
24
25
26
27
28
29
30
31
32
33
34
35
36
37
38
39
40
41
42
43
44
45
46
47
48
49
50
51
52
53
54
55
56
57
58
59
60

Figure 4